References

COENE, W., BENDER, H., LOVEY, F. C., VAN DYCK, D. & AMELINCKX, S. (1985). *Phys. Status Solidi A*, **87**, 483-497.

SCHUBERT, K. (1964). In *Kristallstrukturen Zweikomponentigen Phasen*, p. 92. Berlin: Springer.

TAKEDA, M., VAN TENDELOO, G. & AMELINCKX, S. (1987). *Mater. Res. Bull.* **22**, 1441-1448.

VAN DYCK, D. & COENE, W. (1984). *Ultramicroscopy*, **15**, 29-40.

VAN TENDELOO, G., WOLF R., VAN LANDUYT, J. & AMELINCKX, S. (1978). *Phys. Status Solidi A*, **47**, 539-554.

Acta Cryst. (1988). A**44**, 946-953

Analytic Properties of the Contrast Transfer Function in High-Resolution Electron Microscopy

BY PETER REZ

Center for Solid State Science and Department of Physics, Arizona State University, Tempe, Arizona 85287-1504, *USA*

(*Received* 14 *January* 1988; *accepted* 1 *June* 1988)

Abstract

To calculate high-resolution images it is necessary to convolute the wavefunction generated by scattering from the specimen with the microscope objective-lens wavefront aberration function. This is usually done by a multiplication of the transfer function and the specimen exit-surface wavefunction in reciprocal space followed by a numerical integration over all scattering wave vectors. Examination of the analytic behaviour of the wave-front aberration function in the complex plane shows that, for simple scattering functions, it is possible to perform the integral analytically using the method of stationary phase. Analytic results for the imaging of disordered planes of atoms are compared with fast Fourier transform calculations as a function of defocus. The limitations of stationary-phase integration are also discussed.

The calculation of high-resolution images in electron microscopy can be divided into two parts. The amplitude distribution as a function of scattering wave vector is first calculated using some model for the potential in the specimen and an appropriate theory for electron scattering (Spence, 1980). If the scattering is relatively weak the specimen can be considered as either a strong or a weak phase object (Cowley, 1975). Alternatively, a full dynamical diffraction calculation using either Bloch-wave (Bethe, 1928) or multislice methods (Cowley & Moodie, 1957) could be performed to give the wave function at the exit surface of the crystal.

The second part of the calculation considers the effects of the microscope objective lens and its aberrations in forming the image. This could be done by a convolution in real space but it is more convenient to replace this by a multiplication of the exit-surface wavefunction and the wave-front aberration functions in reciprocal space followed by an integration over all relevant scattering wave vectors (Spence, 1980). The wave-front aberration is an additional phase function $\exp[i\chi(\mathbf{u})]$ where

$$\chi(\mathbf{u}) = (\pi/\lambda)[(C_s/2)\lambda^4 u^4 - f\lambda^2 u^2], \quad (1)$$

where $\mathbf{u}$ is the scattering wave vector, λ is the electron wavelength, f is the defocus and C_s is the lens spherical aberration.

For high-energy electrons, scattering angles are small and the scattering wave vector is assumed to lie in a plane parallel with the specimen surface. It is then more convenient to write the wave-front aberration function in terms of the scattering angle

$$\chi(\theta) = (\pi/\lambda)[(C_s/2)\theta^4 - f\theta^2]. \quad (2)$$

Crystals scatter in directions given by the Bragg angles θ_g for the various crystal planes. The image amplitude is then given by

$$A(\mathbf{r}) = \sum_{\theta_g} \psi(\theta_g) \exp[i\chi(\theta_g)] \exp(2\pi i r\theta_g/\lambda) \quad (3)$$

where $\psi(\theta_g)$ are the complex scattering amplitudes for diffraction from the crystal (Spence, 1980). For single-atom scattering (Chiu & Glaeser, 1975) or scattering by amorphous objects or defects the summation should be replaced by an integration.

$$A(\mathbf{r}) = \int \psi(\boldsymbol{\theta}) \exp[i\chi(\boldsymbol{\theta})] \exp(2\pi i \mathbf{r}\cdot\boldsymbol{\theta}/\lambda)\, \mathrm{d}^2\boldsymbol{\theta}. \quad (4)$$

In the simplest case we can assume that the scattering is given by the weak-phase-object approximation

$$\psi(\boldsymbol{\theta}) = if_e(\boldsymbol{\theta}) \quad (5)$$

where $f_e(\boldsymbol{\theta})$ is the electron scattering factor. The

0108-7673/88/060946-08$03.00 © 1988 International Union of Crystallography

amplitude scattered becomes

$$A(\mathbf{r}) = 1 + i \int f_e(\boldsymbol{\theta}) \exp[i\chi(\boldsymbol{\theta})] \exp(2\pi i \boldsymbol{\theta} \cdot \mathbf{r}/\lambda)\, \mathrm{d}^2\boldsymbol{\theta} \tag{6}$$

and as the scattering is weak the square of the electron scattering factor can be neglected in the expression for the intensity given below.

$$I(\mathbf{r}) = 1 - 2 \int f_e(\boldsymbol{\theta}) \sin[\chi(\boldsymbol{\theta}) + 2\pi \boldsymbol{\theta} \cdot \mathbf{r}/\lambda]\, \mathrm{d}^2\boldsymbol{\theta}. \tag{7}$$

The function $\sin[\chi(\boldsymbol{\theta})]$ is a contrast transfer function. These equations form the basis of the theory for studying the contrast of single atoms or for investigating the properties of the lens using the intensities observed in an image of an amorphous specimen. When scattering in a thin amorphous specimen is used to study the contrast transfer function it is assumed that the electron scattering factor does not change as a function of angle and that atoms are randomly distributed in the specimen. The intensity observed can now be written as

$$I = \int 1 - 2 f_e \sin \chi(\boldsymbol{\theta})\, \mathrm{d}^2\boldsymbol{\theta}. \tag{8}$$

This intensity distribution is studied by examining the diffractogram which is a representation of the power spectrum in reciprocal space. Diffractograms can be taken in an optical bench or by directly computing the Fourier transform from digitized data.

Taking a diffractogram gives an intensity distribution

$$I(\boldsymbol{\theta}) = 4 \sin^2 \chi(\boldsymbol{\theta}) = 2 - 2 \cos[2\chi(\boldsymbol{\theta})]. \tag{9}$$

A typical diffractogram shows a series of bright rings that represent the spatial frequencies that are optimally transferred by the lens (Thon, 1971). In the language of signal processing they are the pass bands suitable for high-resolution imaging and can be found using the conditions that the maxima of $\chi(\boldsymbol{\theta})$ are at $n\pi$. This gives the condition that the focus, f, is equal to $n^{1/2} C_s \lambda$ where n is an odd integer. The condition for the first pass band, $n = 1$, gives a defocus close to the Scherzer focus which we shall call the optimum defocus. Integration over all angles in the diffractogram gives the square of the image variance by Parseval's theorem. Since the work of Frank & Al-Ali (1975) and Erasmus & Smith (1982), the variance has been used directly in computer alignment schemes in high-resolution microscopy to set optimum defocus, and correct for beam-tilt misalignment or astigmatism. By ignoring the constant term and writing the cosine in (9) in terms of exponentials it is possible to integrate $2 \cos 2\chi(\boldsymbol{\theta})$ over all angles directly to give

$$-(\pi/2)(\lambda/C_s)^{1/2} \cos(\pi f^2/\lambda C_s - \pi/4). \tag{10}$$

It is only by assuming that the image was spatially invariant that we were able to perform the integration in a simple fashion. To treat the case of single-atom contrast the integral in (6) has to be performed numerically, usually by fast Fourier transform. Alternatively, the transfer function is approximated as being a constant up to an appropriate cut-off angle which defines an effective aperture. Scherzer (1949) in his classic paper on the imaging of single atoms used such an approach.

Although powerful computers are now widespread, it is of some value to develop analytic approaches as they can very often give new insights into the problem. In this paper the methods of steepest descent and stationary phase (Dennery & Krzywicki, 1967) will be applied to integrals such as those given in (6). Both methods are best suited to integrations where the integral of $g(x)$ can be rewritten as

$$\int g(x)\, \mathrm{d}x = \int \exp f(x)\, \mathrm{d}x. \tag{11}$$

We start by examining the behaviour of the integral as a function of x in the complex plane. As an example we consider the function $\exp(x^2)$. As x increases on the real axis the function tends to infinity. On the imaginary axis it tends to zero and on lines at 45° to the axis the function has constant magnitude. The origin is clearly a minimum when going from $-\infty$ to $+\infty$ and a maximum when going from $-i\infty$ to $+i\infty$. It is, in fact, a saddle point and the imaginary axis is the line of steepest descent through that point. In the method of steepest descents the contour of integration is distorted to follow the steepest-descent line through the saddle point and the integral is approximated by the contribution from the region close to the saddle point. Saddle points are found by setting the first derivative of $f(x)$ equal to zero. If the saddle point is at x_0, the function $f(x)$ is quadratic in $(x - x_0)$ in the neighbourhood of the saddle point, if terms of order $(x - x_0)^3$ and higher-order terms are neglected,

$$f(x) = f(x_0) + f''(x_0)(x - x_0)^2 + O(x - x_0)^3. \tag{12}$$

The integral can be transformed into an integral of the form $\exp -Kx^2$ and the result is

$$\int \exp f(x)\, \mathrm{d}x = (2\pi/A)^{1/2} \exp[f(x_0)] \times \exp[i(\pi - \alpha)/2], \tag{13}$$

where A is the magnitude of $f(x_0)$ and α is its phase.

In the method of stationary phase the contour is made to run along the level lines through the saddle point. Along these lines the variation of phase is at a maximum just as along the lines of steepest descent or ascent there is no change of phase. The integral is then transformed into a Fresnel integral of the form $\int \exp(ikx^2)\, \mathrm{d}x$. The final result of the integration is the same as the expression obtained using the method of steepest descents.

The integral for the square of the variance given in (9) provides a good example of how these methods can be applied. We start by rewriting the integrand

in exponential form

$$\int 2\cos[(\pi C_s/\lambda)(\theta^4-2f\theta^2/C_s)]2\pi\theta\,\mathrm{d}\theta$$
$$=\int 2\pi\{\exp(\mathrm{i}\pi C_s/\lambda)[\theta^4-2f\theta^2/C_s$$
$$-(i\lambda/\pi C_s)\log_e\theta]+\exp(-i\pi C_s/\lambda)$$
$$\times[\theta^4-2f\theta^2/C_s+(i\lambda/\pi C_s)\log_e\theta]\}\,\mathrm{d}\theta. \quad (14)$$

An approximate map of the first exponential term is given as Fig. 1. The contour map in the complex plane is represented as it would be in a micrograph with the hills shaded white and the valleys black. As θ tends to infinity along lines in the complex plane at $3\pi/8$, $7\pi/8$, $11\pi/8$, $15\pi/8$ there are steep hills. Between these hills along lines at $\theta=\pi/8, 5\pi/8, 9\pi/8$ and $13\pi/8$ there are deep valleys. The real and imaginary axes and lines at 45° are the level lies. We require an integration over the real axis from $-\infty$ to $+\infty$ which suggests that stationary-phase integration would be most appropriate. The saddle points are given by the condition

$$\theta^3-f\theta/C_s\mp i\lambda/4\pi C_s\theta=0, \quad (15)$$

where the upper sign represents the expression for the first exponential term and the lower sign the expression for the second exponential term. For the first exponential the saddle points are at

$$\theta=\pm(f/C_s)^{1/2}(1+i\pi\lambda C_s/8f^2). \quad (16)$$

When $\lambda C_s/2<f^2$, the second term can be neglected and the saddle points can be assumed to lie on the real axis. The contribution from the first exponential term at one of the saddle points is

$$I_i=-\pi(f/C_s)^{1/2}\exp(-i\pi f^2/\lambda C_s+i\pi/4)(\lambda/f)^{1/2}. \quad (17)$$

Taking account of the fact that there are two saddle points but that the requirement is for an integral over half the range from 0 to ∞, and then performing the same operation on the second exponential we get

$$I=-(\pi/2)(\lambda/C_s)^{1/2}\cos(\pi f^2/\lambda C_s-\pi/4), \quad (18)$$

which is the same as was found by simple integration.

We shall now consider the integral for the amplitude given as (6). For simplicity we shall only treat one-dimensional scattering from an atom. This could arise in practice if disordered planes of heavy atoms were stacked in a well defined sequence among ordered planes of light atoms, with the planes normal to the specimen surface (see Fig. 2). Scattering in a direction normal to the planes gives superlattice reflections corresponding to the repeat distance of the heavy-atom planes, while scattering in a direction lying in the plane is the same as scattering from an amorphous material. For the purposes of this paper an atom will be represented as a single Gaussian with a half width of about 0·5 Å. Summation over four Gaussians is equivalent to the Doyle & Turner (1969) parameterization of the electron scattering factor. In fact an examination of the Doyle & Turner (1969) parameters shows that only two Gaussians are needed to represent most atoms to about 10% accuracy. The fact that the electron scattering factors do not have the correct asymptotic form for high scattering angles need not concern us in any discussion on high-resolution microscopy as these angles will be cut off by the transfer function. If the half width of the atom is R the electron scattering factor is

$$f_e(\theta)=C\exp(-b\theta^2)$$

where

$$b=(R\pi/\lambda)^2(\log_e 2)^{-1}. \quad (19)$$

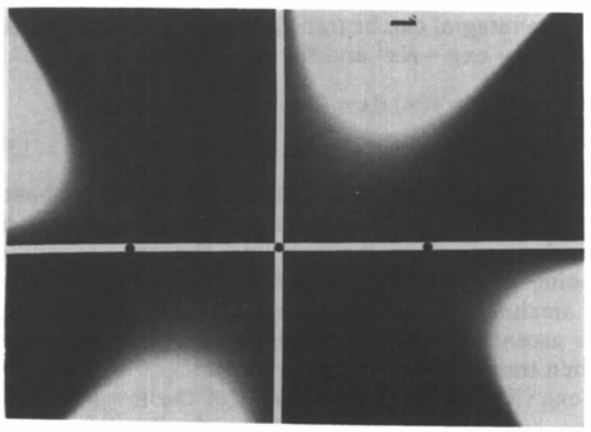

Fig. 1. Map of the function $\exp(i\pi/\lambda)(C_s\theta^4-2f\theta^2-i\lambda\log_e\theta/\pi)$ for a defocus of 400 Å and a C_s of 1 mm at 100 kV. The saddle points are marked with white dots and the integration contour is the x axis. Peak white is 0·5. The bar corresponds to 10 mrad.

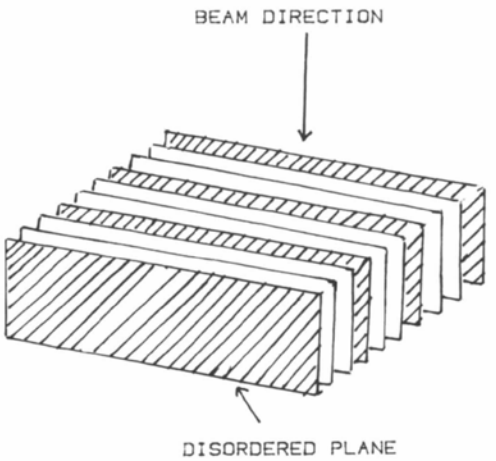

Fig. 2. Diagram showing a possible arrangement of disordered planes of heavy atoms that might give rise to one-dimensional atomic diffuse scattering.

Incorporating this equation in (6), we can see that putting in the atomic scattering factor is equivalent to making the defocus complex. The effective imaginary defocus for the atom is

$$R^2\pi/\lambda \log_e 2$$

which is 30 Å for an atom of half-width 0·5 Å and would be about 120 Å for an atom of half-width 1 Å. These values are very small compared with the optimum defocus and can usually be neglected except near Gaussian focus. If we neglect the factor i which multiplies the expression, the amplitude becomes the Fourier transform of the wave-front aberration function with an appropriate complex defocus

$$-iA(r)/C = \int \exp[(i\pi/\lambda)(C_s\theta^4/2 - f\theta^2 + 2r\theta)]\,\mathrm{d}\theta. \quad (20)$$

In the weak-phase-object approximation, the intensity is twice the imaginary part of the above expression. The integral of (20) can also be written as a Fourier transform and in the next section we shall compare results obtained using stationary phase with numerical fast Fourier transforms of the wave-front aberration function.

All the subsequent calculations refer to a microscope with an objective lens C_s of 1 mm operating at 100 kV. The first passband in defocus occurs at $f = (C_s\lambda)^{1/2}$, which is 608 Å. Microscopes operating at 200 and 400 kV with the same value for optimum defocus would have objective-lens spherical aberration coefficients of 1·5 and 2·0 mm respectively. These values are physically reasonable for microscopes operating today though the highest-resolution microscopes have C_s of order 1 mm at 400 kV. The optimum

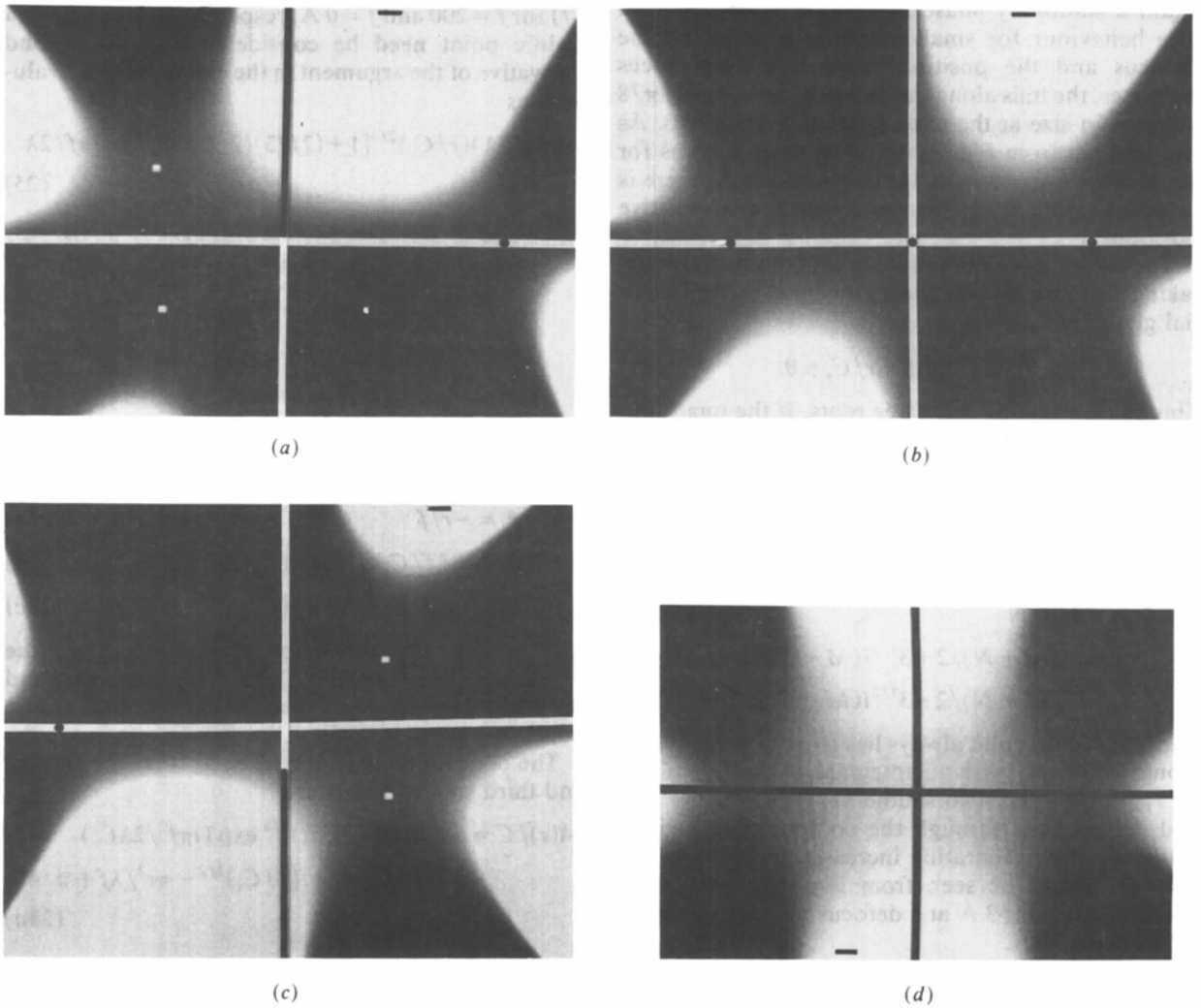

Fig. 3. Maps of the function $\exp[(i0{\cdot}5\pi/\lambda)(C_s\theta^4 - 2f\theta^2 + 4r\theta)]$ for (*a*) $r = -3$ Å, (*b*) $r = 0$ Å, (*c*) $r = 3$Å for 100 kV scattering from atoms of half-width 0·5 Å. Peak white is 5·0 and the dots mark the saddle points. The contour of integration is the x axis and the bar corresponds to 10 mrad. (*d*) Map of the phase of the function for $r = 0$ Å. Peak white in this map is 15·0 and black is −25·0.

defocus value is then 405 Å. If we consider the various microscopes with the same value of optimum defocus then the only variable that changes is the magnitude of the characteristic scattering angle. If the scattering wave vector is expressed in Glaeser units (Hawkes, 1980) $(C_s\lambda^{3/4})^{-1}$, then the characteristic scattering angle is $(\lambda/C_s)^{1/4}$. As far as the lens transfer function is concerned an angle of 10 mrad at 100 kV becomes equivalent to 8·1 mrad at 200 kV and 6·7 mrad at 400 kV.

To evaluate the amplitude given by (20) using the method of stationary phase we must first examine the behaviour of the function in the complex plane. At large values of θ the function should be dominated by the spherical aberration term. Just as in the case of the image variance, there will be mountains along lines going through $3\pi/8$, $7\pi/8$, $11\pi/8$ and $15\pi/8$ with valleys along lines going through $\pi/8$, $5\pi/8$, $9\pi/8$ and $13\pi/8$. The level line is the real axis and again a stationary-phase integration is appropriate. The behaviour for small angles is affected by the defocus and the position terms. As the defocus increases, the hills along the lines from $3\pi/8$ to $11\pi/8$ increase in size at the expense of the other hills. As can be seen from Fig. 3, which shows the maps for positions −3, 0, +3 Å at a defocus of 600 Å, there is a mirror symmetry going from negative to positive positions.

The positions of the saddle points can be found by taking the derivatives of the argument of the exponential given by

$$\theta^3-(f/C_s)\theta+r/C_s=0. \tag{21}$$

This cubic equation has three roots. If the quantities M and N are defined as

$$M=[-r/2C_s+(r^2/4C_s^2-f^3/27C_s^3)^{1/2}]^{1/3} \tag{22a}$$

$$N=[-r/2C_s-(r^2/4C_s^2-f^3/27C_s^3)^{1/2}]^{1/3} \tag{22b}$$

then the roots of the equation are

$$\theta_1=M+N \tag{23a}$$

$$\theta_2=-(M+N)/2+3^{1/2}i(M-N)/2 \tag{23b}$$

$$\theta_3=-(M+N)/2-3^{1/2}i(M-N)/2. \tag{23c}$$

The first saddle point always lies close to the real axis along which we wish to integrate. When $r^2/4C_s^2>f^3/27C_s^3$, the other two saddle points lie off the axis and do not pass through the contour. For a given value of r their separation increases with decreasing defocus as can be seen from Fig. 4 which shows function maps for 3 Å at a defocus of 1000, 800, 600, 400, 200 and 0 Å.

If $r^2/4C_s^2<f^3/27C_s^3$ these other two saddle points are close together and lie on the integration contour. This can be seen in the contour image for 0 Å in Fig. 3(*b*) and the contour image for a defocus of 1000 Å in Fig. 4(*a*). The saddle points are very apparent in the phase map for 0 Å as given in Fig. 3(*d*) which should be compared with the corresponding amplitude contour image in Fig. 3(*b*). Table 1 gives the value of r which separates these two regions as a function of defocus.

Approximate limiting solutions can be derived in both these cases. When $r^2/4C_s^2\gg f^3/27C_s^3$, the saddle points are given by

$$\theta_1=-(r/C_s)^{1/3}[1+(f/3)(2/C_sr^2)^{1/3}] \tag{24a}$$

$$\theta_2=\tfrac{1}{2}(r/C_s)^{1/3}[1-(f/3)(2/C_sr^2)^{1/3}] + i(3^{1/2}/2)(r/C_s)^{1/3}[1-(f/3)(2/C_sr^3)^{1/3}] \tag{24b}$$

$$\theta_3=\tfrac{1}{2}(r/C_s)^{1/3}[1+(f/3)(2/C_sr^3)^{1/3}] - i(3^{1/2}/2)(r/C_s)^{1/3}[1+(f/3)(2/C_sr^3)^{1/3}]. \tag{24c}$$

In the limit of large r they are all at $|\theta|=(r/c_s)^{1/3}$ in directions π, $\pi/3$, $-\pi/3$. In Fig. 4 the trend towards this limiting solution is apparent in Figs. 4(*e*) and (*f*) for $f=200$ and $f=0$ Å, respectively. Only the first saddle point need be considered and the second derivative of the argument in the exponential is evaluated as

$$(i\pi C_s/2\lambda)(r/C_s)^{2/3}[1+(2f/3)(2/C_sr^2)^{1/3}]-i\pi f/2\lambda. \tag{25}$$

The integral can now be written approximately as

$$\begin{aligned} iA(r)/C=2\{\lambda/[(C_sr^2)^{1/3}-f]\}^{1/2}&\exp(i\pi/4)\\ &\times\exp\{i(i\pi C_s/2\lambda)\\ &\times[(r/C_s)^{4/3}-2(f/C_s)(r/C_s)^{2/3}\\ &-4r(r/C_s)^{1/3}]\}. \end{aligned} \tag{26}$$

The other limit when $f^3/27C_s^3\gg r^2/4C_s^2$ is significant when r is small or f is large.

$$\theta_1=-r/f \tag{27a}$$

$$\theta_2=+(f/C_s)^{1/2}[1-\tfrac{1}{2}(C_s/f)^{3/2}(r/C_s)] \tag{27b}$$

$$\theta_3=-(f/C_s)^{1/2}[1+\tfrac{1}{2}(C_s/f)^{3/2}(r/C_s)]. \tag{27c}$$

The second derivatives of the argument of the exponential are $+i\pi r/2\lambda(C_s/f)^{3/2}$ for the second and third saddle points and $-i\pi f/2\lambda$ for the first saddle point.

The contributions to the integral from the second and third saddle points are

$$\begin{aligned} iA(\mathbf{r})/C=4(\lambda/r)^{1/2}&(f/C_s)^{3/4}\exp(i\pi f^2/2\lambda C_s)\\ &\times\cos[(2\pi r/\lambda)(f/C_s)^{1/2}-\pi r^2/\lambda f+\pi/4] \end{aligned} \tag{28a}$$

and from the first saddle point it is

$$iA(\mathbf{r})/C=2(\lambda/f)^{1/2}\exp(-3\pi ir^2/\lambda f-i\pi/4). \tag{28b}$$

In our investigation of the method we did not use these approximate results but went back to (23) to

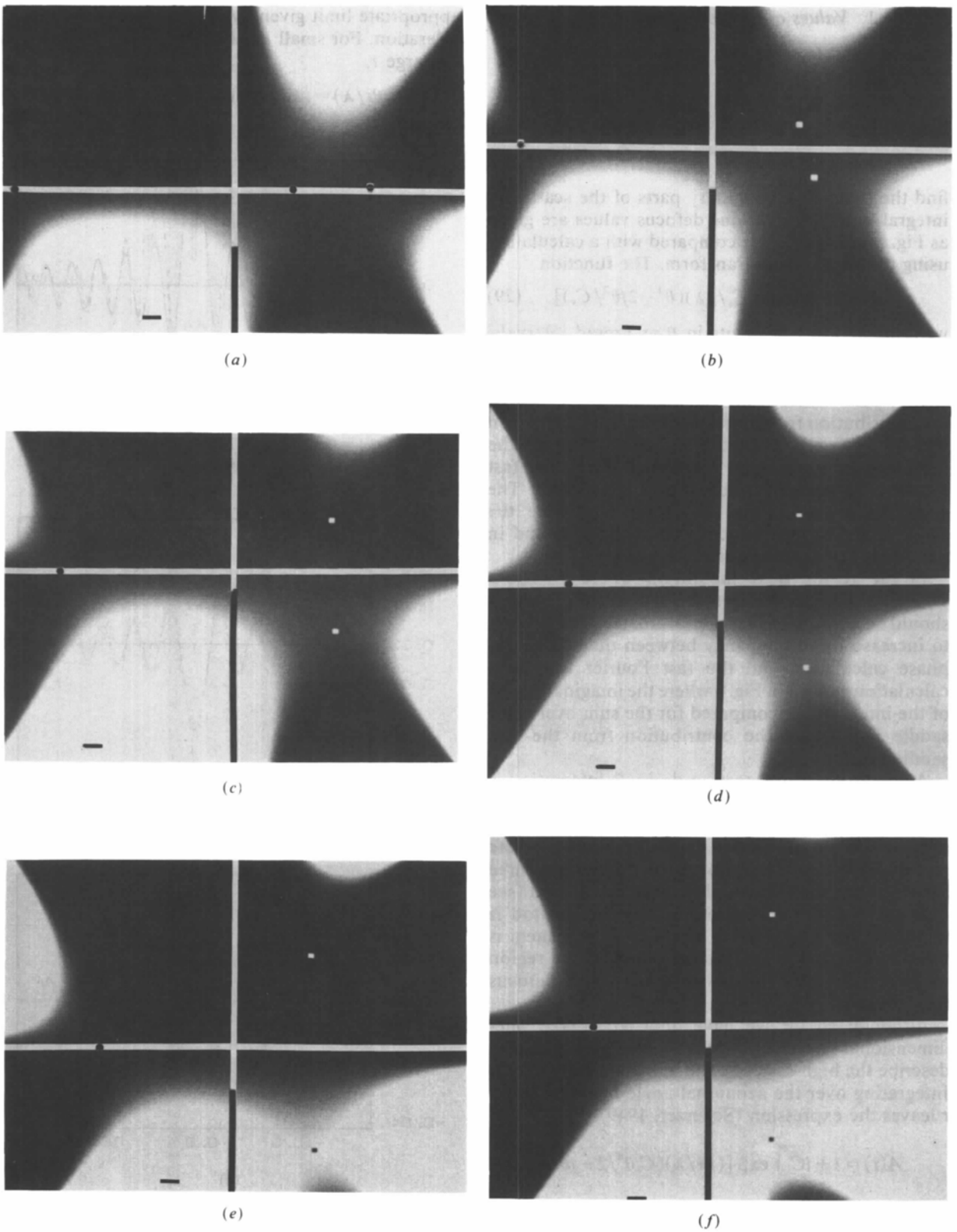

Fig. 4. Maps of the function $\exp[(i0{\cdot}5\pi/\lambda)(C_s\theta^4-2f\theta^2+4r\theta)]$ for 100 kV electrons, atom half-width of 0·5 Å, $r=3$ Å and defocus, f, (*a*) 1000 Å, (*b*) 800 Å, (*c*) 600 Å, (*d*) 400 Å, (*e*) 200 Å, (*f*) 0 Å. Peak white is 5·0, the contour of integration is the x axis and the dots mark the saddle points. The bar corresponds to 10 mrad.

Table 1. *Values of position r where* $r^2 = 4f^3/27C_s$

f defocus (Å)	r position (Å)
200	0·34
400	0·97
600	1·7
800	2·75
1000	3·84

find the roots. The imaginary parts of the scattering integral in (20) for various defocus values are given as Fig. 5 where they are compared with a calculation using the fast Fourier transform. The function

$$g(\boldsymbol{\theta}) = \exp[(i\pi C_s/2\lambda)(\theta^4 - 2f\theta^2/C_s)] \quad (29)$$

was sampled at 256 points in θ at 1 mrad intervals. It was found that increasing the number of points or changing the sampling interval did not appreciably change the result. All the calculations in Fig. 5 used the contribution from one saddle point. In the region where $r^2/4C_s > f^3/27C_s^3$ the differences between the stationary-phase integral (solid lines) and the fast Fourier transform (broken lines) are small. The stationary-phase integral does not reproduce the small higher-order frequency components found in the direct Fourier transform calculation.

In the region near the origin where $r^2/4C_s^2 < f^3/27C_s^3$ the contributions from all three saddle points should be added together. Unfortunately this appears to increase the discrepancy between the stationary-phase calculation and the fast Fourier transform calculation as seen in Fig. 6 where the imaginary parts of the integrals are compared for the sum over three saddle points and the contribution from the first saddle point.

A condition of the steepest-descents integration is that the contour should dip into a steep valley between saddle points. The analogous condition for stationary-phase integration is that the phase should oscillate rapidly. This condition is not properly met when three saddle points along the real axis are considered (see Fig. 3*d*) and this is the reason why the method is unreliable for small values of r. The disagreement is more serious for large defocus values as the region where $r^2 < 4f^3/27C_s$ increases in size with defocus (see Table 1).

Although so far we have only considered one-dimensional scattering the theory can be modified to describe the high-resolution imaging of single atoms. Integrating over the azimuthal angle between $\boldsymbol{\theta}$ and $\mathbf{r}$ leaves the expression (Scherzer, 1949)

$$A(\mathbf{r}) = 1 + iC \int_0^\infty \exp[(i\pi/\lambda)(C_s\theta^4/2 - f\theta^2)] \times J_0(2\pi\theta r/\lambda)\theta \, d\theta. \quad (30)$$

This could be put in the form required for stationary-phase or steepest-descent integration by taking the asymptotic form of the Bessel function in the appropriate limit given by the range of r under consideration. For small r, $J_0(2\pi\theta r/\lambda)$ is of order 1 and for large r,

$$J_0(2\pi\theta r/\lambda) \simeq (\lambda/\pi^2\theta r)^{1/2} \cos(2\pi\theta r/\lambda - \pi/4).$$

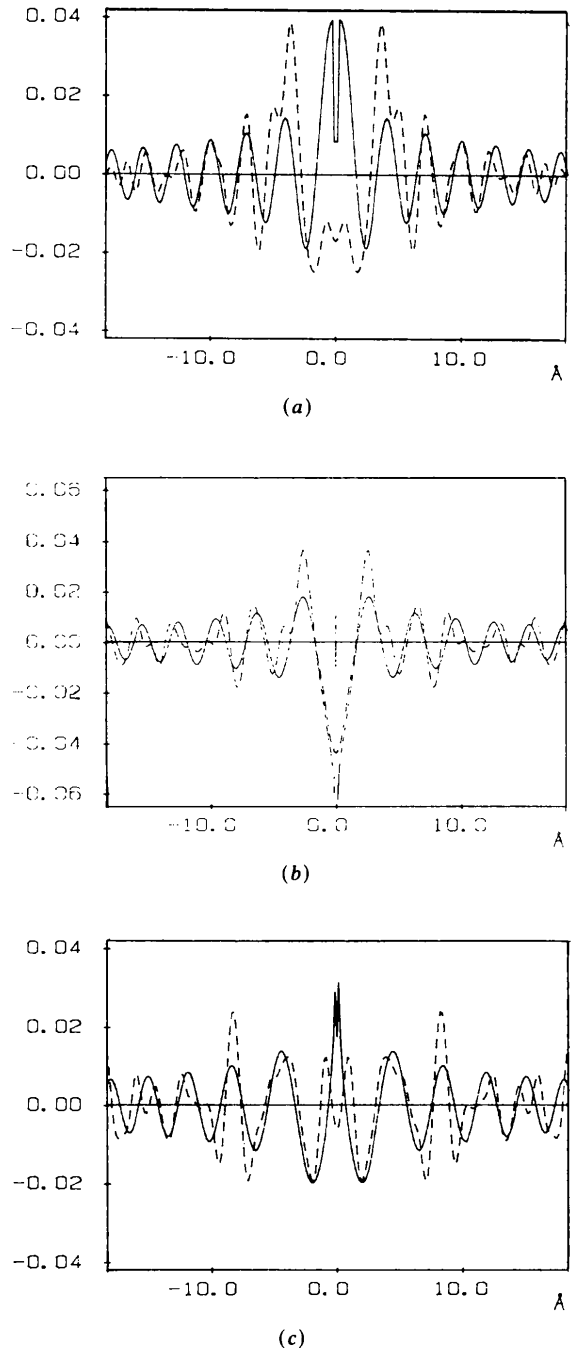

Fig. 5. Comparison of imaginary parts of the amplitude integral for (*a*) 1000 Å, (*b*) 600 Å, (*c*) 200 Å calculated by the stationary-phase method with one saddle point (solid lines) and the numerical fast Fourier transform (broken lines). The accelerating voltage is 100 kV, the atom half-width is 0·5 Å and the C_s is 1 mm.

The integral analogous to (20) becomes

$$-iA(\mathbf{r})/C = (\lambda/\pi^2 r)\exp(\mp i\pi/4) \times \int_{-\infty}^{\infty} \exp[(i\pi C_s/2\lambda)(\theta^4 - 2f\theta^2/C_s \pm 4\theta r/C_s - 2i\lambda \log_e \theta/\pi C_s)]\,\mathrm{d}\theta.$$

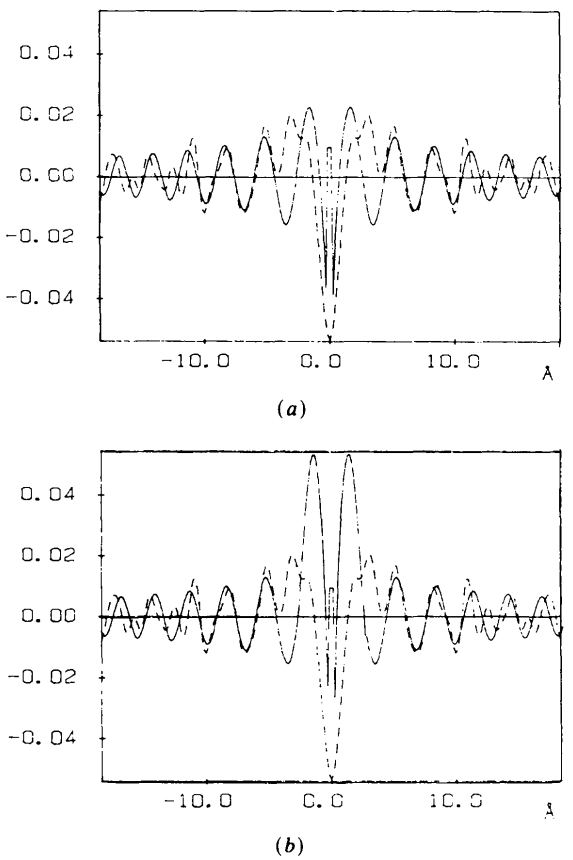

Fig. 6. Comparison of the imaginary part of the amplitude integral calculated by stationary phase with (*a*) contribution from one saddle point, (*b*) contributions from three saddle points for a defocus, *f*, of 800 Å. The stationary-phase integrations are shown as solid lines, the fast Fourier transform results are shown as broken lines. The accelerating voltage is 100 kV, the atom half-width is 0·5 Å and the C_s is 1·0 mm.

In practice this might not be that different from the integral that we have already evaluated as the $\log_e \theta$ term is slowly varying. Another possible approach would be to leave the integral over azimuthal angle to be evaluated after the integral over θ. It is, however, questionable whether this would be analytically tractable in the larger-r limit.

In conclusion we have shown that integrals over the electron-microscope wave-front aberration function can be performed analytically (with reasonable accuracy) by the method of stationary phase. We have applied the stationary-phase method to calculations of the image variance and to the calculation of the amplitude observed from the one-dimensional scattering of atoms. In both cases the stationary-phase calculation is in good agreement with other calculations provided the saddle points that contribute to the integral are not too close to each other. In practice it has meant that the amplitude calculations are only reliable when $r^2 > 4f^3/27C_s$ and only one saddle point contributes to the integral. By assuming a Gaussian representation for atomic scattering we have shown that atoms can be incorporated in imaging theory as a complex defocus. For any reasonable atomic size the imaginary part of the defocus is of order 20–50 Å. This would suggest that under weak-phase-object conditions differences between different atoms would show up best near Gaussian focus.

References

BETHE, H. (1928). *Ann. Phys. (Leipzig)*, **87**, 55-129.

CHIU, W. & GLAESER, R. M. (1975). *J. Microsc.* **103**, 33-54.

COWLEY, J. M. (1975). *Diffraction Physics.* Amsterdam: North-Holland.

COWLEY, J. M. & MOODIE, A. F. (1957). *Acta Cryst.* **10**, 609-619.

DENNERY, P. & KRZYWICKI, A. (1967). *Mathematics for Physicists.* New York: Harper and Row.

DOYLE, P. A. & TURNER, P. S. (1968). *Acta Cryst.* **A24**, 390-397.

ERASMUS, S. & SMITH, K. C. A. (1982). *J. Microsc.* **127**, 185-199.

FRANK, J. & AL-ALI, L. (1975). *Nature (London)*, **256**, 376-379.

HAWKES, P. W. (1980). *Ultramicroscopy*, **5**, 67-70.

SCHERZER, O. (1949). *J. Appl. Phys.* **20**, 20-29.

SPENCE, J. C. H. (1980). *Experimental High Resolution Microscopy.* Oxford Univ. Press.

THON, F. (1971). *Electron Microscopy in Materials Science*, edited by U. VALDRÈ & A. ZICHICHI, pp. 570-590. New York: Academic Press.